CHAPTER 7

RESULTS AND DISCUSSION

The first results presented will be on the SGT data reduction performed on High Pressure Turbine Blades of various engines. The following results will show the correlation in natural frequencies and mode shapes obtained for analytical modeling using contact elements versus the results data obtained from the SGT data reduction. The last section will present the results on the correlation between the analytical vibratory stress prediction and the vibratory stress results obtained from the SGT data reduction.

7.1 Strain Gage Test Data Reduction Results

This section will present the results from the SGT data reduction performed on the PWC Engine 1, PWC Engine 2 and PWC Engine 3 engines. The results will be presented in tables, one for each engine and in three main sections: resonance results, damping extraction results and stress results.

7.1.1 Resonance results

The resonance results presented in the following tables represent only the highest peak strain values for each mode and strain gage location during the data reduction. Since only the maximum strain values are of concern, only the corresponding run number (Run column) and strain gage location (SG column) are presented. The natural frequency values may differ for different strain gage location since the strain gages are placed on different blades. Turbine blades have little differences between them that would slightly shift the natural frequencies, although the mode and harmonic excitation are the same. In addition, the crystal orientation would create differences in the natural frequency values. The Mode column presents which mode (ex: M2) is in resonance with

which excitation harmonic (ex: 1H for first harmonic). The frequency (Frequency column) and the engine rotating speed (N2 or Ng) associated with the resonance are given. The modes and excitations presented in the following tables are the only ones that were in resonance within the engine speed operating range. The natural frequencies are normalized to the first frequency value of the tables.

Table IV

PWC Engine 1 Resonant Frequencies

Airfoil RPM

Mode	SG	Run	Frequency	N2
M2-1H	3E	8485/1/11	1.0	35222
M4-2H		8485/1/11	1.558	33321
M2-1H	1D	8485/1/11	1.0	35231
M4-2H		8485A/1/11	1.564	33517
M2-1H	12G	8485A/1/11	1.0	35235
M4-2H		8485A/1/11	1.538	32906
M2-1H	5F	8485A/1/11	1.016	35766
M4-2H		8485/1/11	15456	33134
M2-1H	7M	8485A/1/11	1.0	35332
M4-2H		8485A/1/11	1.503	32215

Fixing RPM

Mode	SG	Run	Frequency	N2
M2-1H	8A	8485A/1/11	1.016	35786
M4-2H		8485A/1/11	1.535	32852
M2-1H	9C	8485/1/11	1.006	35456
M4-2H		8485/1/11	1.535	32852

The results for the natural frequencies of the other engine models are presented in APPENDIX 2.

7.1.2 Modal damping extraction results

The total damping values presented below are separated by engine models, modes and harmonic excitations. The total damping values were extracted from the SGT data reduction presented in section 3.2. The curve fitting was performed and the minimum R^2 value was of 0.912. To complete the damping analysis, a correlation has to be done in function on the wetted area of the blade and the excitation harmonic. It is believed that the mechanical damping and the aerodynamical damping is function of the wetted area of the blade. Although, there are many other parameters, which are functions of the damping, it was chosen to observe this particular one. The extracted damping is in the logarithmic decrement form and transformed to zeta form (ration between the damping and the critical damping) form using the following equation:

$$\zeta = \frac{\delta}{\sqrt{\delta^2 + 4\pi^2}} \tag{7.1}$$

Table V

PWC Engine 1 Modal damping

Mode	M2		M3		M4	
Excitation	2H		2H		2H	
Harmonic	2nd		2nd		2nd	
Damping	Dec. Log.	Zeta (%)	Dec. Log.	Zeta (%)	Dec. Log.	Zeta (%)
Data	0.0223	0.355%	0.0121	0.193%	0.0163	0.259%
	0.0240	0.382%	0.0128	0.204%	0.0186	0.296%
	0.0240	0.382%			0.0153	0.243%
	0.0242	0.385%			0.0133	0.212%
	0.0304	0.484%			0.0194	0.309%
Average	0.0250	0.398%	0.0125	0.198%	0.0164	0.264%
Q value	125.6		252.5		189.4	
Variance	9.77E-06	2.48E-07	2.45E-07	6.21E-09	1.79E-05	1.54E-07

The results for the modal damping of the other engine models are presented in APPENDIX 3.

The damping correlation was made in regards to the excitation harmonic and the blade airfoil wetted area (Figure 16).

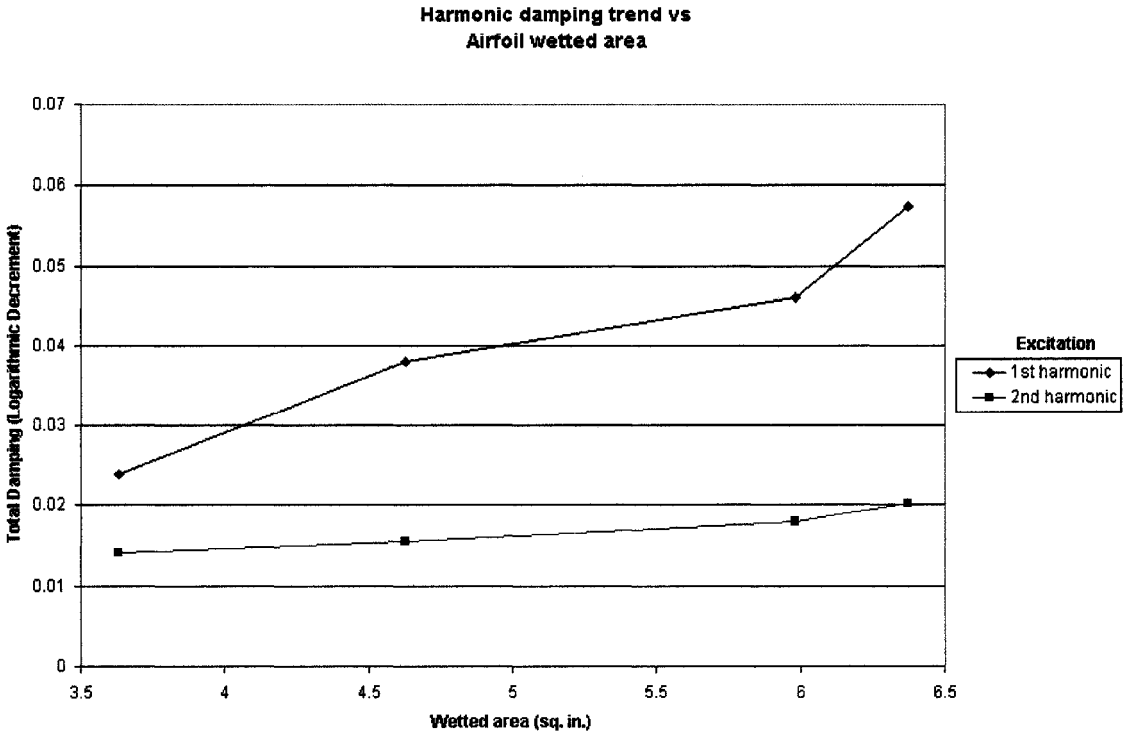

Figure 16 Harmonic damping trend vs. Airfoil wetted area

The correlation between the total damping and the blade airfoil wetted area show that they are linear with each other. The higher the wetted area, the higher the total damping value will be. Furthermore, the 2nd harmonic excitation total damping is much lower than the 1st harmonic excitation. This would explain why we see such high vibratory stresses for 2nd harmonic excitation.

7.1.3 Experimental vibratory stress results

The following tables present the stress results from the SGT data reduction of the PWC Engine 1, PWC Engine 2 and PWC Engine 3. The waterfall strain (WF strain) peak values are obtained directly from the resonance point of the waterfall plot (Figure 4). The overall strain (OA strain) is obtained by the square root sum of the strain values of the whole frequency range for a given resonance speed. The engine order strain (EO strain) is the peak value obtained from the whole engine order excitation speed and within a certain frequency band. All the strain values are given in micro strain (10^{-6}) format. The blade strain gage location metal temperature (T metal) was obtained from a steady thermal analysis. The Young's modulus (E) was obtained from the material properties of each blade at the given metal temperature and strain gage orientation.

Table VI

PWC Engine 1 Vibratory Stress

E6211B6

Airfoil			RPM	ksi	ksi	ksi
Mode	**SG**	**Frequency**	**N2**	**WF stress**	**OA stress**	**EO stress**
M2-1H	3E	1.0	35222	0.6304	1.2555	0.1799
M4-2H		1.558	33321	11.7580	11.9439	11.8257
M2-1H	1D	1.0	35231	2.6215	3.0175	0.2644
M4-2H		1.564	33517	1.0654	1.6468	3.0482
M2-1H	12G	1.0	35235	7.8369	8.5780	6.3823
M4-2H		1.538	32906	5.2755	5.8280	13.4422
M2-1H	5F	1.016	35766	1.5157	3.3161	2.5611
M4-2H		15456	33134	10.9549	11.2905	0.0000
M2-1H	7M	1.0	35332	4.7775	6.3161	19.2286
M4-2H		1.503	32215	2.4487	4.6595	13.7954

Table V (continued)

Fixing		Hz	RPM	ksi	ksi	ksi
Mode	**SG**	**Frequency**	**N2**	**WF stress**	**OA stress**	**EO stress**
M2-1H	8A	1.016	35786	0.9460	2.1165	2.9464
M4-2H		1.535	32852	0.6582	1.6300	1.3487
M2-1H	9C	1.006	35456	0.7692	2.1214	0.3901
M4-2H		1.535	32852	2.0652	2.5273	2.0789

Due to data storage discrepancies, the stress values for the PWC Engine 2 HPT blade could not be found. This was remedied to be best accuracy by using the stress value from the certification reports.

The results for the vibratory stress of the other engine models are presented in APPENDIX 4.

7.1.4 Discussion on the strain gage data reduction results

The resonances were identified for each CT or HPT blade of various engines. Using the resonance points, the modal damping was extracted.

The modal damping values were presented in the logarithmic decrement form and a zeta form for each engine CT or HPT blades. It was noticed that the higher the harmonic excitation, the lower the total modal damping value would be. Furthermore, the smaller the wetted volume of the blade is, the lower the total modal damping. This is an important fact, especially when these damping values will be used for new engines development with similar blade sizes and shapes. The variance for some engine was very good while others seem to have high difference for the same mode. This can be explained with the quality of the SGT data. If the signal is noisy or the modes are coupled, it is difficult to fit a SDOF curve on the test signal.

The strain values at each identified resonance were extracted. By multiplying the strain with the Young's Modulus, which is function of the metal temperature and orientation of the strain gage, the vibratory stress values at each resonance were found. The values of stress seem to be consistent in regards to different modes and harmonic excitations. Since these values were obtained experimentally, it is assumed that they can be used for analytical comparison.

7.2 Results of the Updated Boundary Conditions Analyses

The initial study presented in the primary results and the convergence study were performed on the PWC Engine 1 HPT blade. This blade represents most of the blades analyzed in this study and therefore, the findings can be extrapolated to the other engine models. The analytical results of all the CT or HPT blades studied are also presented.

7.2.1 Comparison between the current and the new analyses

The natural frequencies obtained from the new analysis with contact elements compared to the strain gage values were found to be in good agreement. The natural frequencies computed for modes 1 and 2 were found to have an average error range of 5 to 8% while modes 3 and 4 were found to have an average error range of 0 to 2%. The mode shapes were found to be identical between the current and the new analyses (using same displacement scale) (Figure 17 & 18).

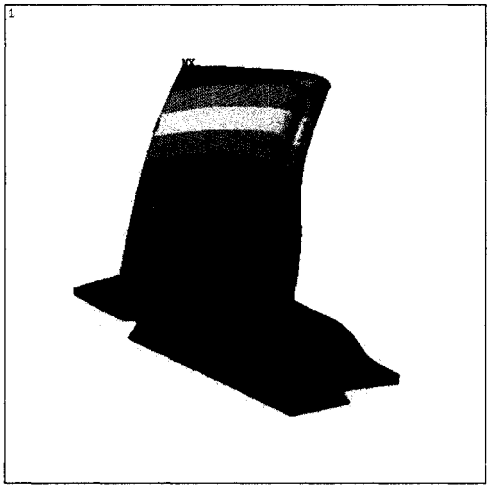

Figure 17 Current analysis mode shape

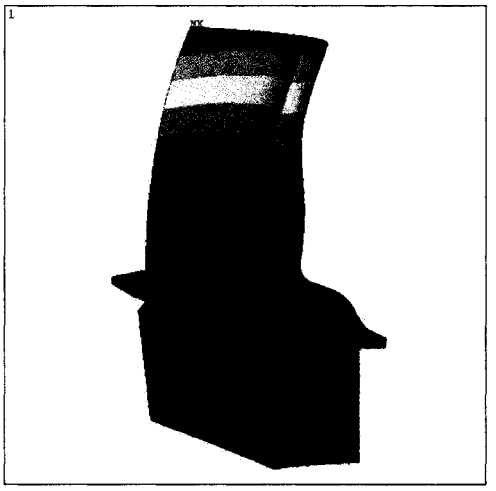

Figure 18 New analysis mode shape

Furthermore, the stress levels in the fir-tree area were compared of the current (see Figure 8) and the new analyses using contact elements (Figure 19) were compared.

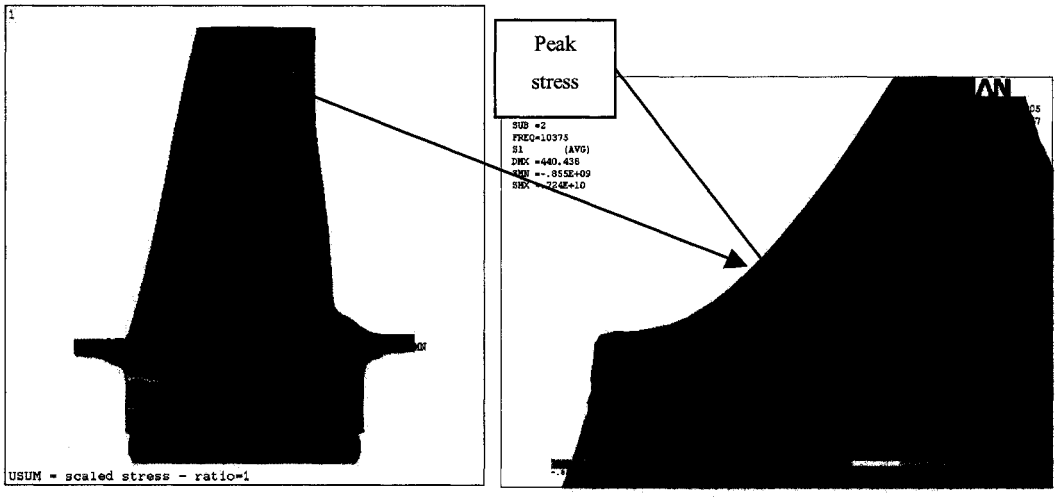

Figure 19 Blade stress in the fir-tree area (Inside the airfoil's cooling pocket)

The stress level in the fir-tree area for the new analysis was found to be lower by a factor of approximately 40% compared to the current analysis. It can therefore be assumed that the new analysis with contact elements will predict stress levels with more accuracy than

will the current analysis. Finally, it was confirmed that the contact face was enlarged by 5% during the pre-stress static analysis (Figure 20).

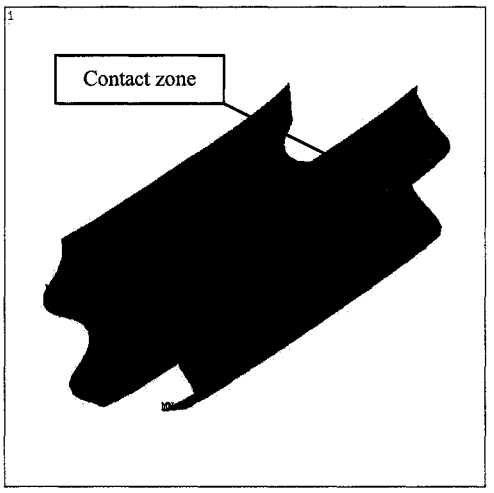

Figure 20 Contact face width

This result proves that the blocked contact face does not reflect the phenomenon, and therefore should not be used in such analyses.

7.2.2 Convergence study

A study was performed to determine the contact element parameter values, which would yield the best convergence results. This study was performed on multiple models of blades to ensure reproducibility for the next designs. The first parameter studied was the friction coefficient (MU) (Figure 21).

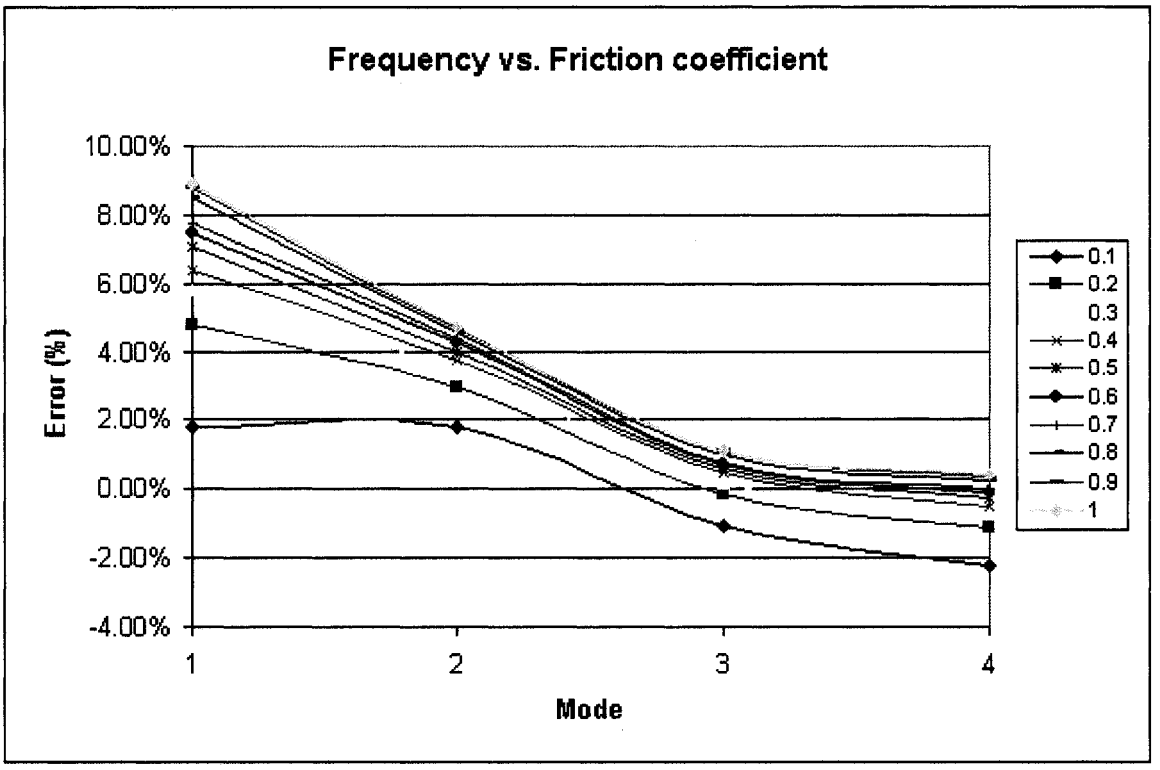

Figure 21 Frequency error vs. friction coefficient

A convergence was found between the values 0.9 to 1. This showed that the model was stable, and that convergence could be achieved. It was noticed that the higher the friction coefficient value, the higher the error for modes 1 and 2, while modes 3 and 4 tended to remain the same. This seems to indicate that mode 1 and 2, i.e. first bending and first torsion, are much more susceptible to sliding friction than the higher order modes (mode 3 and 4), although this phenomenon needs to be further evaluated. Therefore, there is an optimum friction coefficient value for each mode. In this case, for mode 1 and 2, a friction coefficient value between 0 and 0.1 would minimise the error, while a friction coefficient close 1.0 would minimise the error for mode 3 and 4.

The second parameter studied was the normal contact stiffness factor (FKN) (Figure 22).

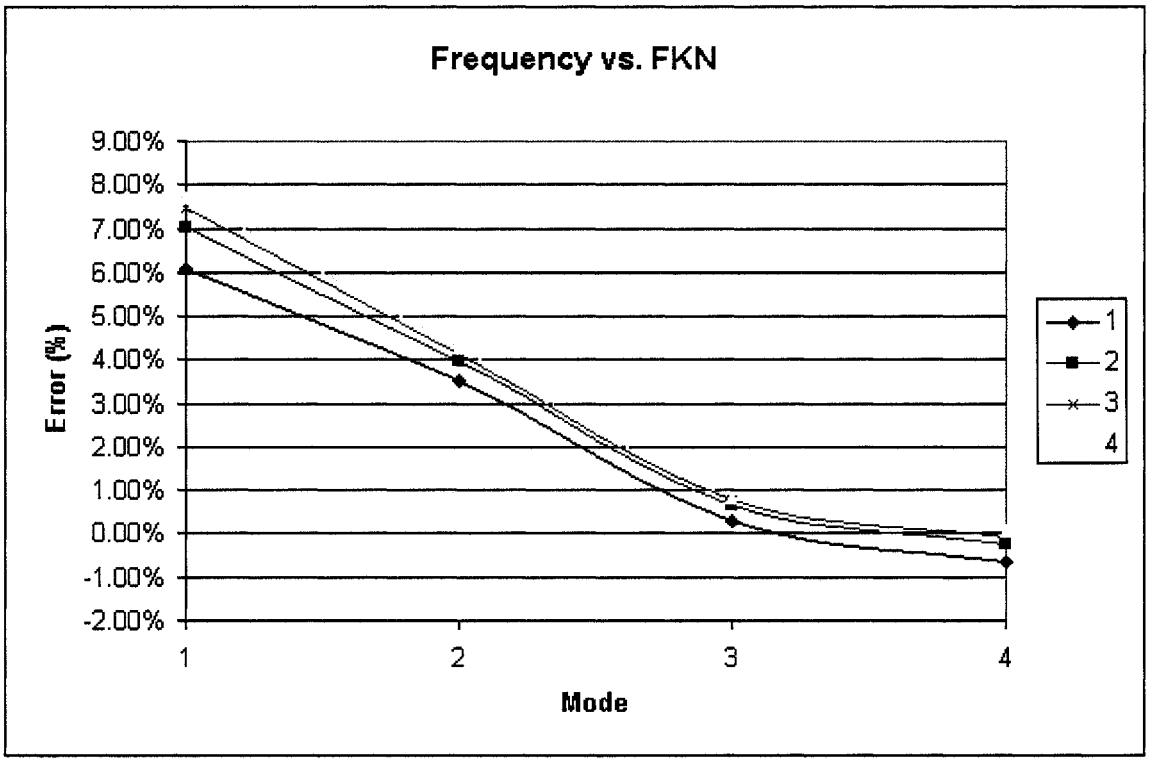

Figure 22 Frequency vs. Normal contact stiffness factor

It was noticed that the error tends to proportional to the normal contact stiffness factor. This indicates that the higher the factor, the less the penetration that occurs and therefore there is an increase in natural frequency. Convergence is achieved when very little or no penetration occurs between the blade and the disc. This phenomenon has to be studied more thoroughly by performing experimental penetration tests.

The third parameter studied was the penetration tolerance factor (Figure 23).

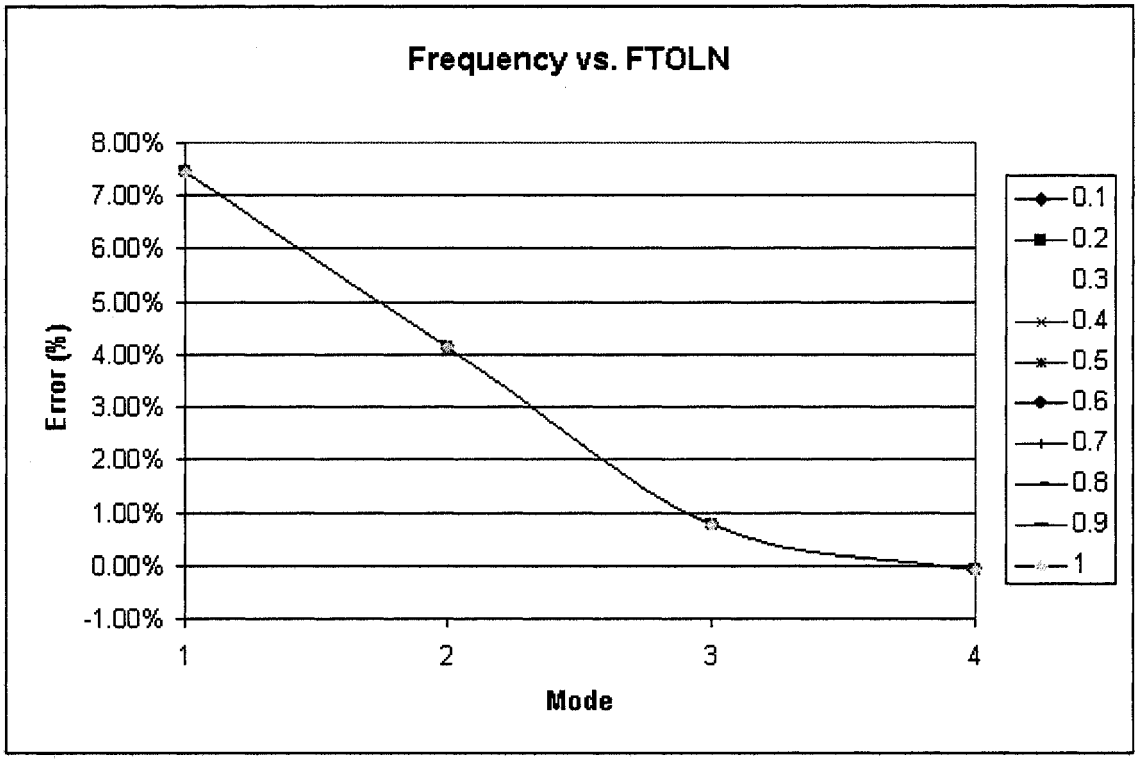

Figure 23 Frequency vs. Penetration tolerance factor

It was observed that the penetration tolerance factor had no effect on natural frequencies. This could be explained by the fact that the analysis predicts a penetration smaller than the allowable value (factor value multiplied by the depth of the underlying solid). Therefore, if the factor is larger than the penetration, the parameter will have no effect on the results. However, the factor cannot be too great or else the model convergence will not be obtained.

The fourth and fifth parameters were studied simultaneously. The ratio between the static and dynamic friction coefficient (FACT) and the slip rate decay coefficient (DC) were varied at the same time during the study (Figure 24).

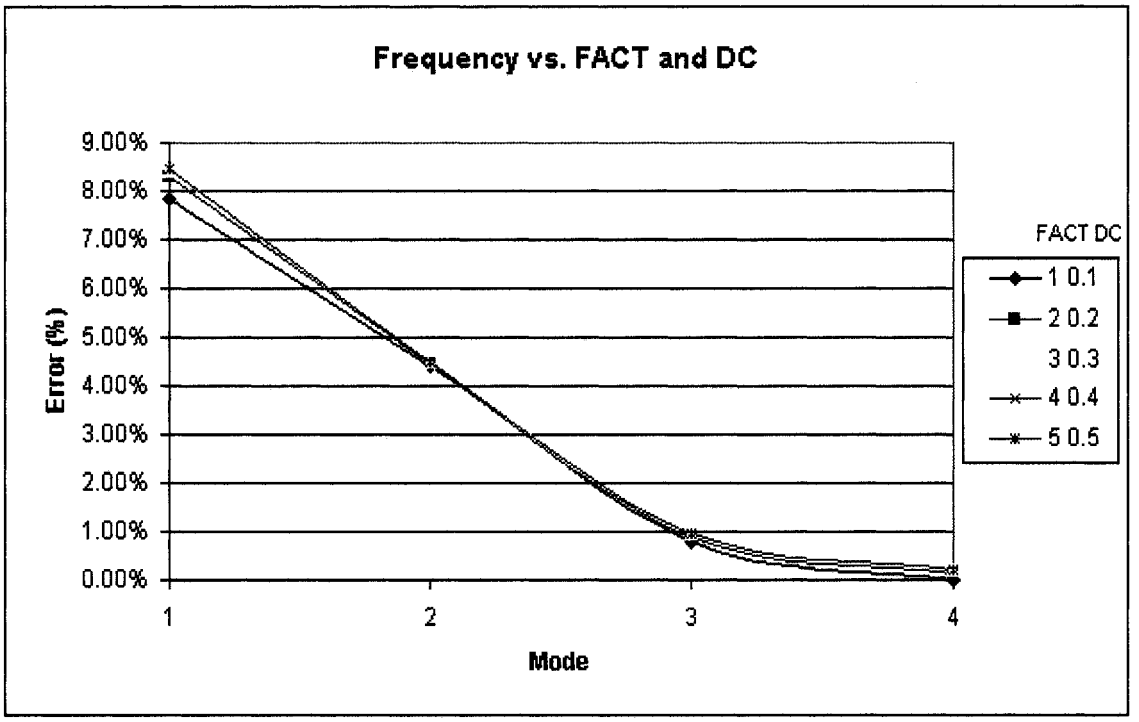

Figure 24 Frequency vs. Ratio between the static and dynamic friction coefficient and the slip rate decay coefficient

The ratio between the static and dynamic friction coefficient and the slip rate decay coefficient were found to have very little effect on the results. This seems to indicate that there is a low slip rate, and thus the parameters have little effect on the friction coefficient.

7.2.3 Analytical results using contact elements modal analysis

The PWC Engine 1 HPT, PWC Engine 2 HPT and PWC Engine 3 CT blades were analyzed using contact elements as boundary conditions between the fixing of the blade and the disc. The natural frequencies of the first four (4) modes were extracted and compared to the average value of the natural frequencies extracted from the strain gage test data. The analyses were performed at either the maximum speed or the resonant speed conditions. The natural frequencies have been normalized to the experimental

value (SGT) of the first mode. Based on the convergence study, the following contact element variable values were used to determine the natural frequencies for each of the engine models blade:

- Dynamic coefficient of friction (MU) = 0.1;
- Normal stiffness factor (FKN) = 1;
- Penetration tolerance factor (FTOLN) = 1;
- Ratio between the static and dynamic coefficient (FACTOR) = 1;
- Slip rate decay coefficient (DC) = 0.1.

7.2.3.1 PWC Engine 1 HPT Blade Natural Frequency Prediction

Table VII

PWC Engine 1 HPT Blade Natural Frequency Comparison @ 35200 RPM

@ 35200 RPM				
Mode	**SGT**	**Std. Dev.**	**ANSYS**	**Error**
1	1.0	0.27%	1.043	4.35%
2	2.428	0.78%	2.506	3.23%
3	3.237	0.38%	3.360	3.80%
4	3.647	0.72%	3.609	1.04%

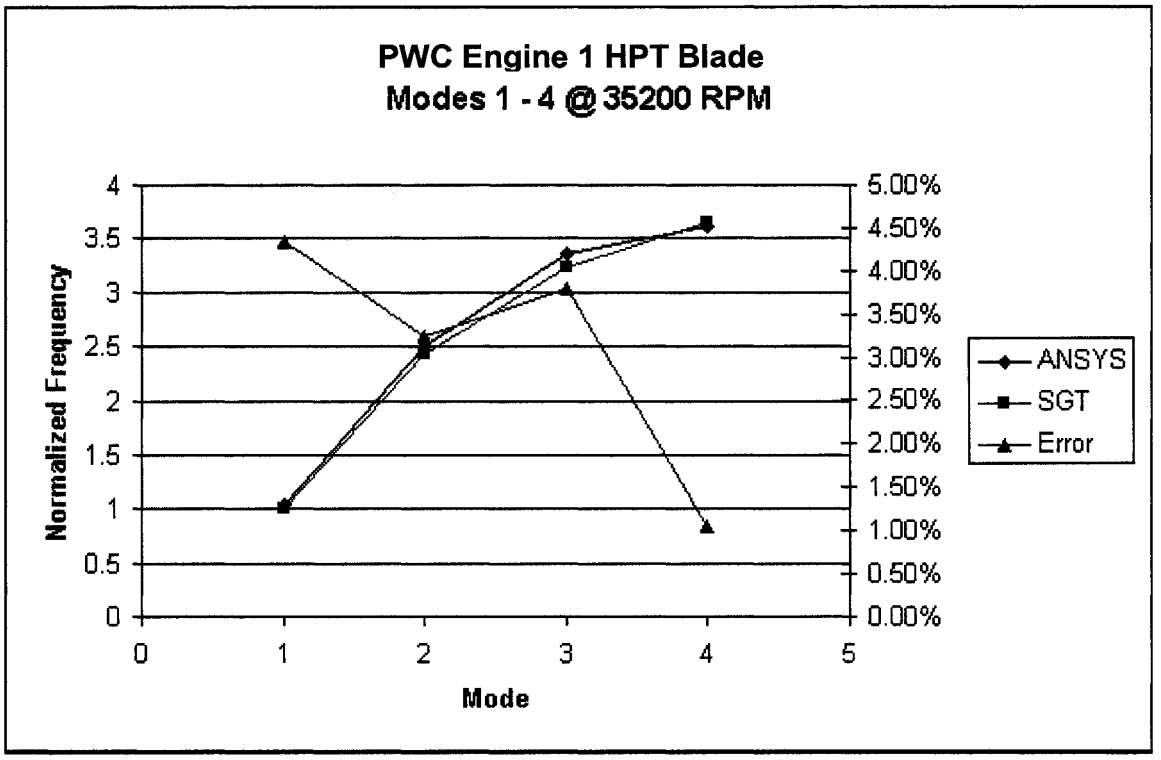

Figure 25 PWC Engine 1 HPT Blade Natural Frequency Comparison @ 35200 RPM

Table VIII

PWC Engine 1 HPT Blade Natural Frequency Comparison @ 33000 RPM

@ 33000 RPM				
Mode	**SGT**	**Std. Dev.**	**ANSYS**	**Error**
1	1.0	1.35%	1.050	4.98%
2	2.405	0.62%	2.479	3.08%
3	3.283	1.11%	3.415	4.01%
4	3.683	1.28%	3.679	0.13%

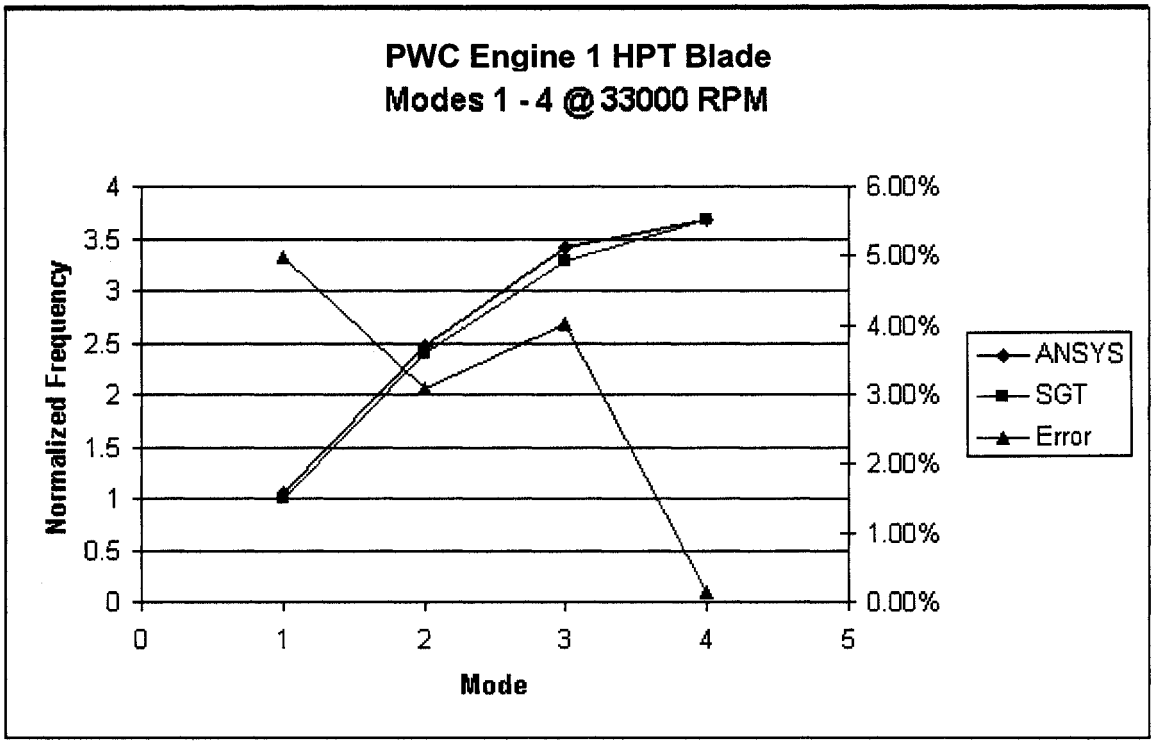

Figure 26 PWC Engine 1 HPT Blade Natural Frequency Comparison @ 33000 RPM

The correlation between the natural frequencies on the analytical solution and the SGT data was within 5% error margin. It was determined that the analytical solution overestimated the first two modes while underestimated the third and fourth modes. The differences can be explained in the geometry used for the analytical compared to the one used during the SGT.

7.2.3.2 PWC Engine 2 HPT Blade Natural Frequency Prediction

Table IX

PWC Engine 2 HPT Blade Natural Frequency Comparison @ 33289 RPM

@ 33289 RPM				
Mode	SGT	Std. Dev.	ANSYS	Error
1	1.0	1.20%	0.956	4.38%
2	2.317	0.17%	2.286	1.37%
3	2.8	7.86%	2.879	2.83%
4	3.8	0.80%	3.675	3.29%

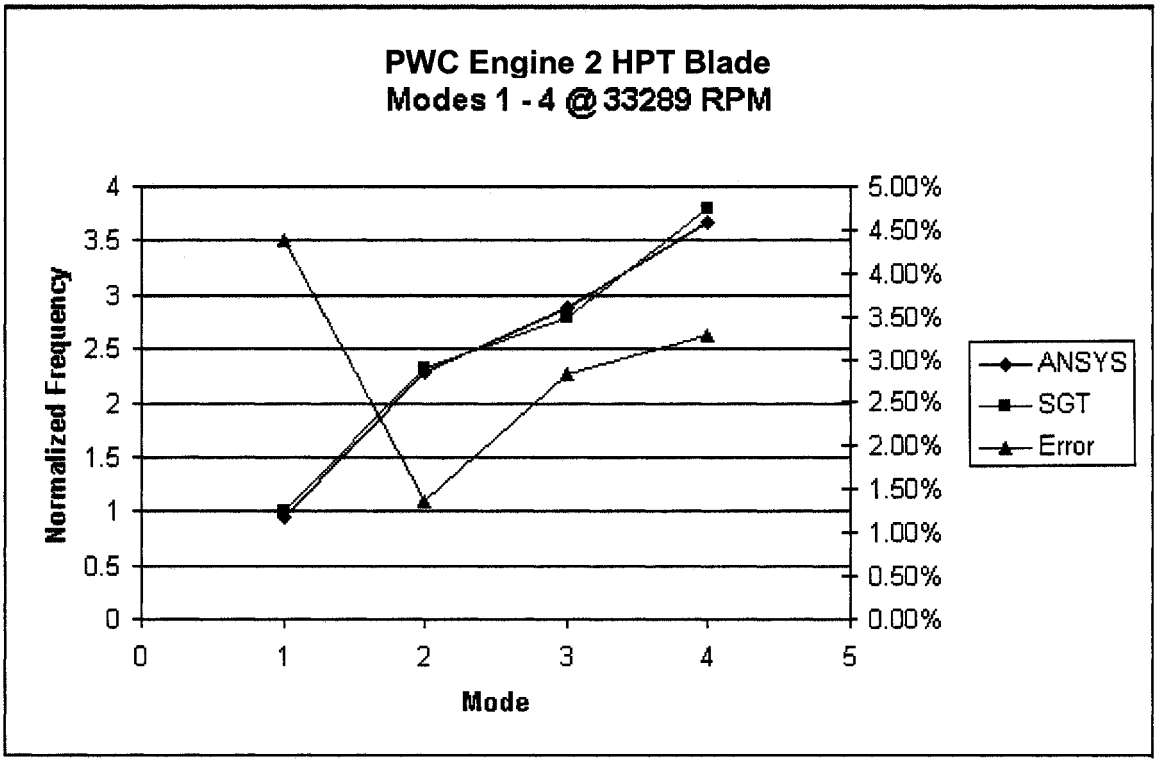

Figure 27 PWC Engine 2 HPT Blade Natural Frequency Comparison @ 33289 RPM

Table X

PWC Engine 2 HPT Blade Natural Frequency Comparison @ 30000 RPM

@ 30000 RPM				
Mode	SGT	Std. Dev.	ANSYS	Error
1	1.0	3.0%	0.962	3.85%
2	2.440	4.47%	2.404	1.48%
3	2.837	1.18%	2.912	2.65%
4	3.821	2.08%	3.678	3.74%

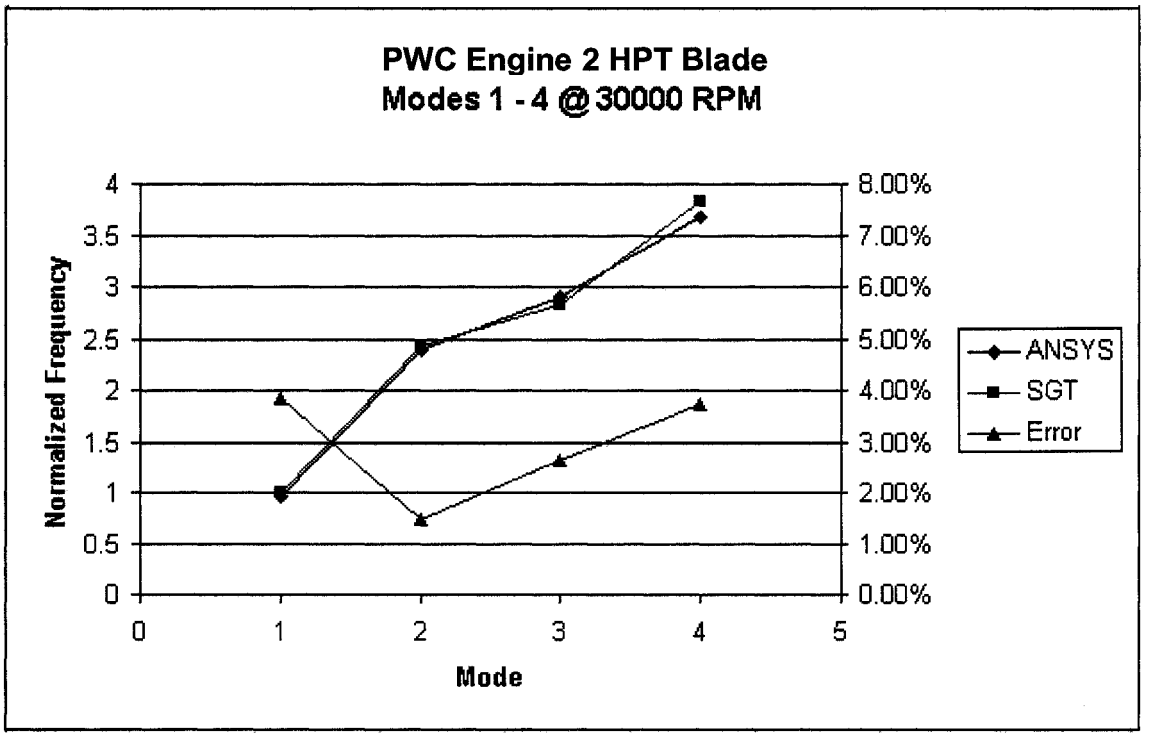

Figure 28 PWC Engine 2 HPT Blade Natural Frequency Comparison @ 30000 RPM

The correlation between the natural frequencies on the analytical solution and the SGT data was within 5% error margin. It was determined that the analytical solution overestimated the first mode only while underestimated the second, third and fourth

modes. The differences can be explained in the geometry used for the analytical compared to the one used during the SGT. Also, a higher dynamic coefficient of friction could be used to increase the natural frequencies determined by the modal analysis.

7.2.3.3 PWC Engine 3 CT Blade Natural Frequency Prediction

Table XI

PWC Engine 3 CT Blade Natural Frequency Comparison @ 43000 RPM

@ 43000 RPM				
Mode	**SGT**	**Std. Dev.**	**ANSYS**	**Error**
1	1.0	2.36%	0.993	0.65%
2	2.164	0.31%	2.255	4.16%
3	2.799	2.96%	2.931	4.74%
4	3.214	0.79%	3.204	0.29%

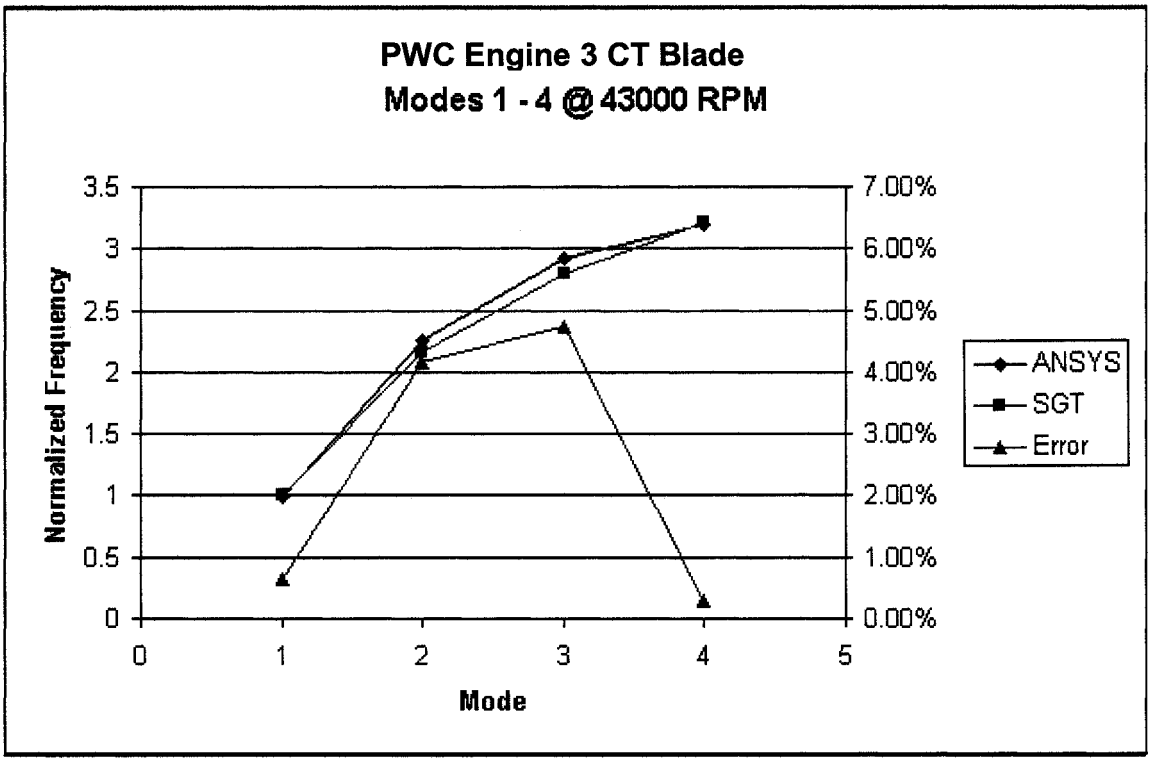

Figure 29 PWC Engine 3 CT Blade Natural Frequency Comparison @ 43000 RPM

Table XII

PWC Engine 3 CT Blade Natural Frequency Comparison @ 36000 RPM

@ 36000 RPM				
Mode	SGT	Std. Dev.	ANSYS	Error
1	1.0	0.90%	1.005	0.54%
2	2.231	1.79%	2.331	4.48%
3	2.854	7.25%	2.994	4.88%
4	3.266	0.25%	3.325	1.81%

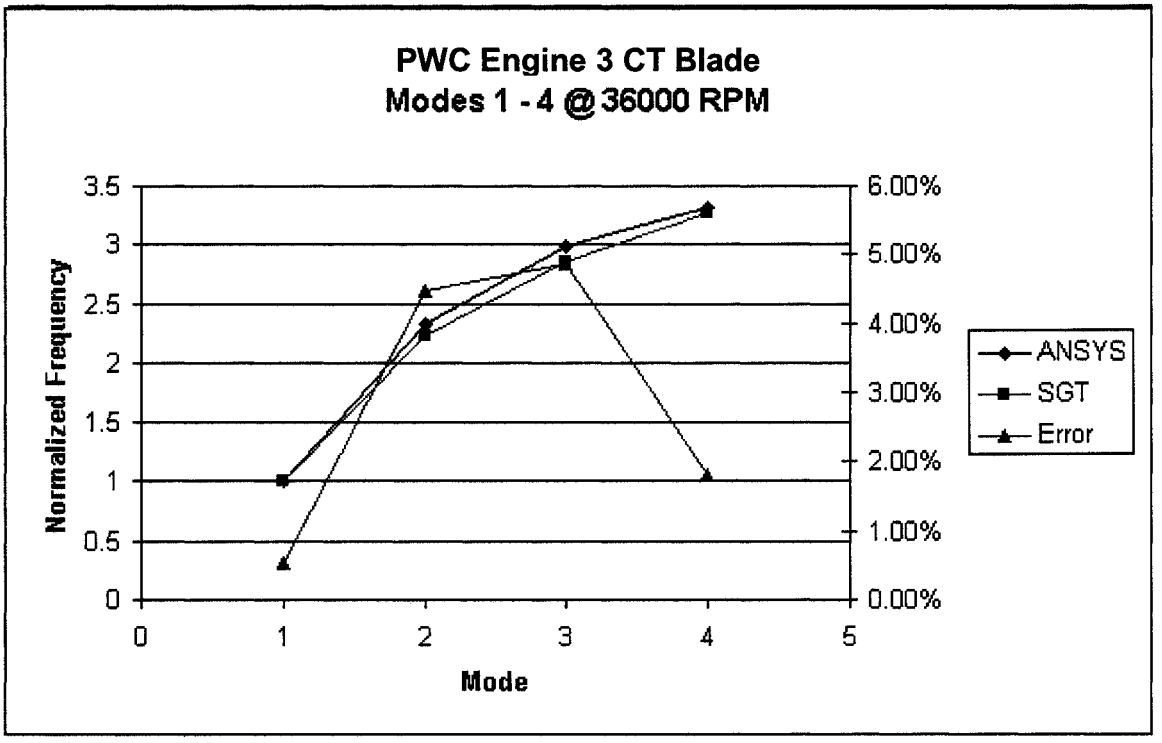

Figure 30 PWC Engine 3 CT Blade Natural Frequency Comparison @ 36000 RPM

The correlation between the natural frequencies on the analytical solution and the SGT data was within 5% error margin. It was determined that the analytical solution overestimated the second mode only while underestimated the first, third and fourth

modes. The differences can be explained in the geometry used for the analytical compared to the one used during the SGT.

7.3 Experimental Tests Results

The experimental testing was not performed with great success. The main deficiency was the excitable frequency range performed by the high-frequency speaker. The JBL Professional Series Model No. 2425 speaker coupled to a Model No. 2306 horn was only able to excite a frequency range from 3500 to 8000 Hz. The excited frequency range was determined by plotting the frequency response of the microphone during the testing period (Figure 31).

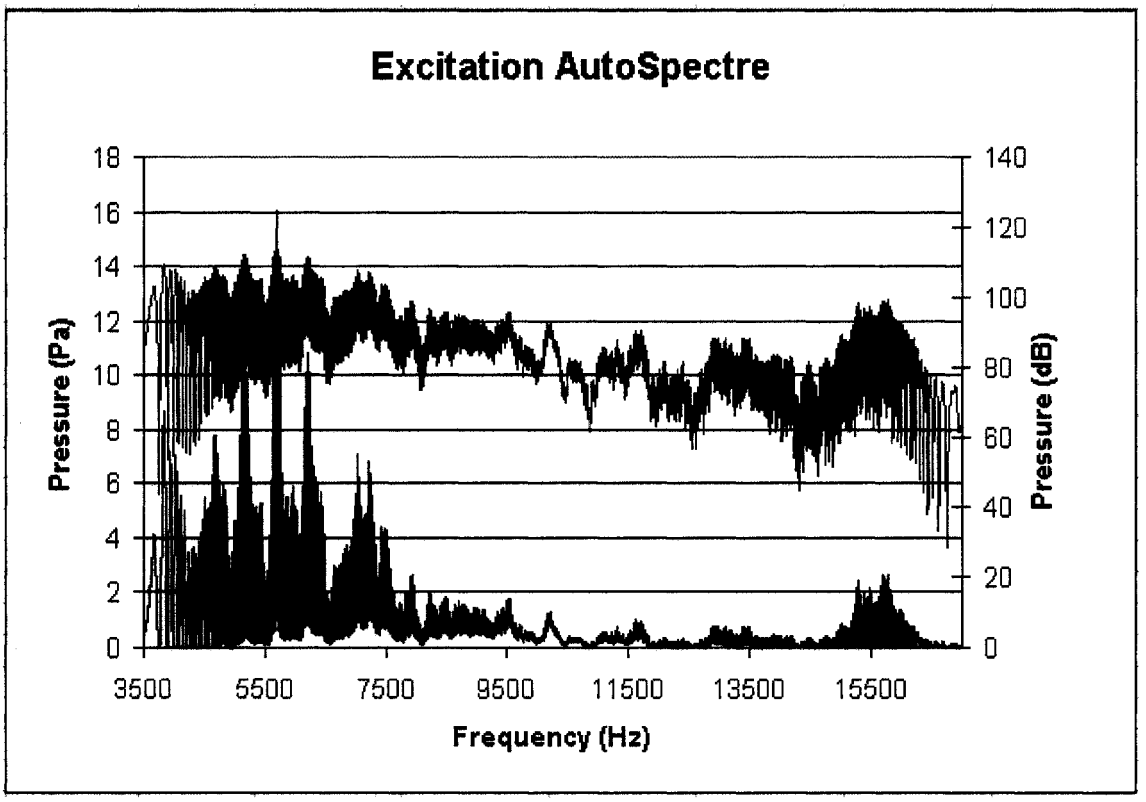

Figure 31 Excitation Autospectrum for excited frequency range

The FEM analysis showed the 4th mode of the Blade used for testing had a natural frequency of 16638 Hz, which is more than double the excited frequency range. Therefore, the results for the 2nd, 3rd and 4th modes will be very questionable. Furthermore, the coherence signal showed weaknesses at multiple frequencies due to the lack excited frequency range.

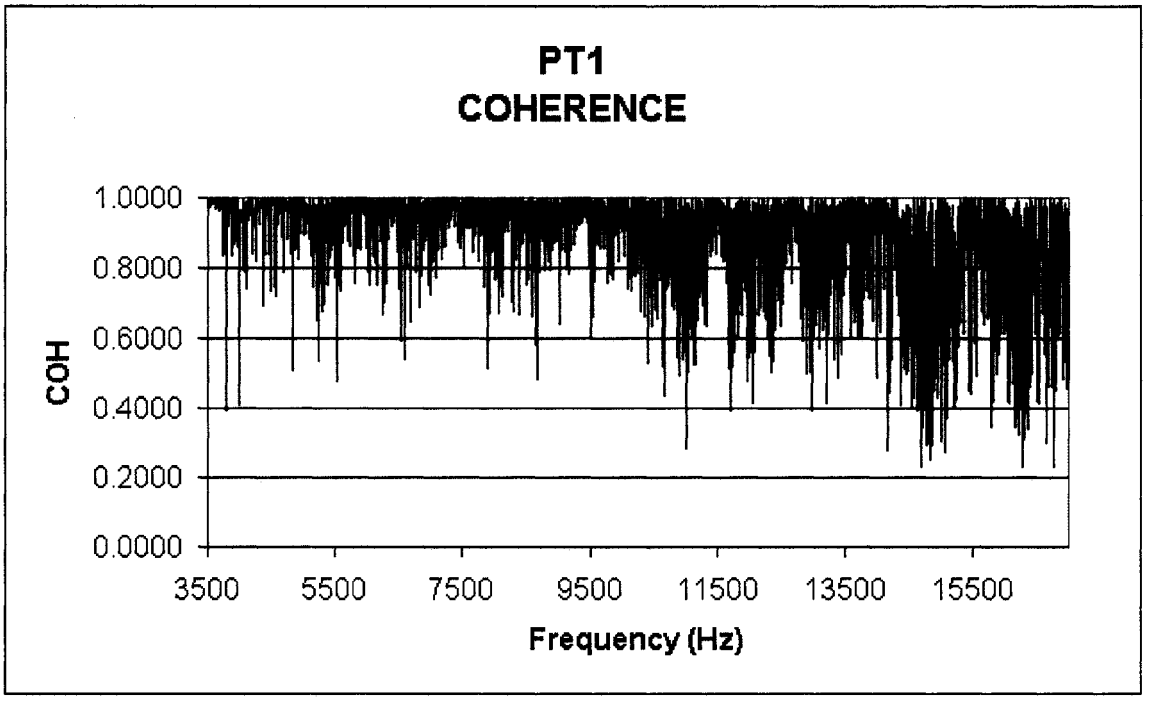

Figure 32 Example of a Coherence signal

To determine the mode shape and damping for each mode, the values (positive or negative) from the F.R.F real signal are taken for each location and natural frequency (Figure 33).

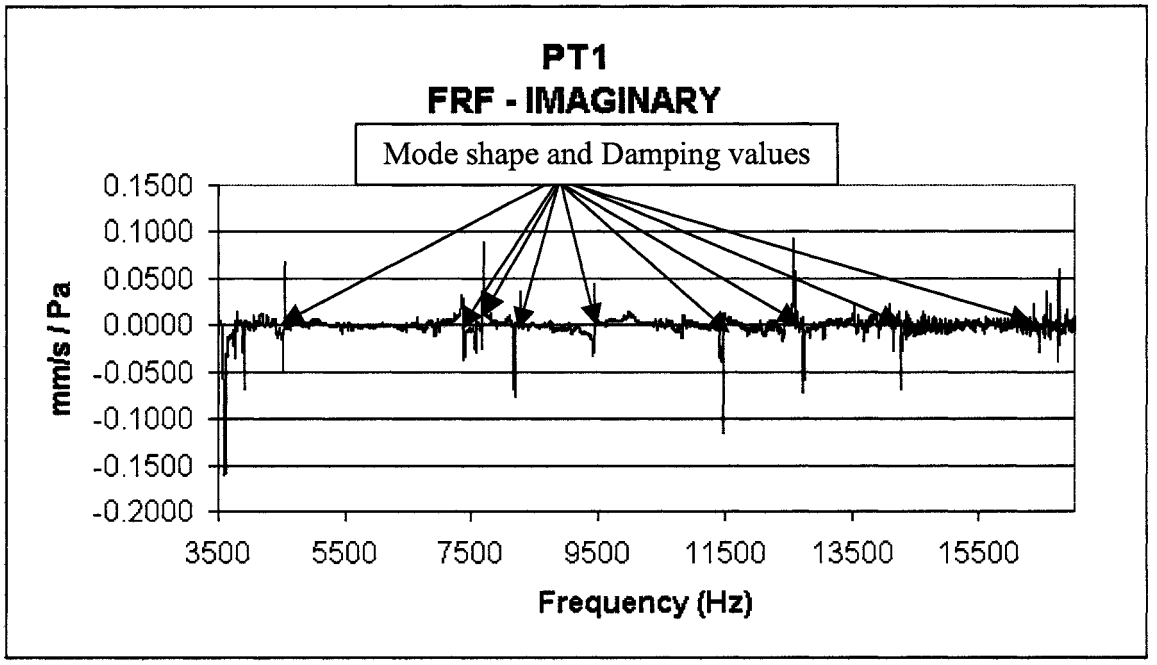

Figure 33 Example F.R.F. signal Imaginary part for mode shape and damping determination

The natural frequencies were determined by finding the intersection between the F.R.F. signal imaginary part and the null axis for every location (Figure 34).

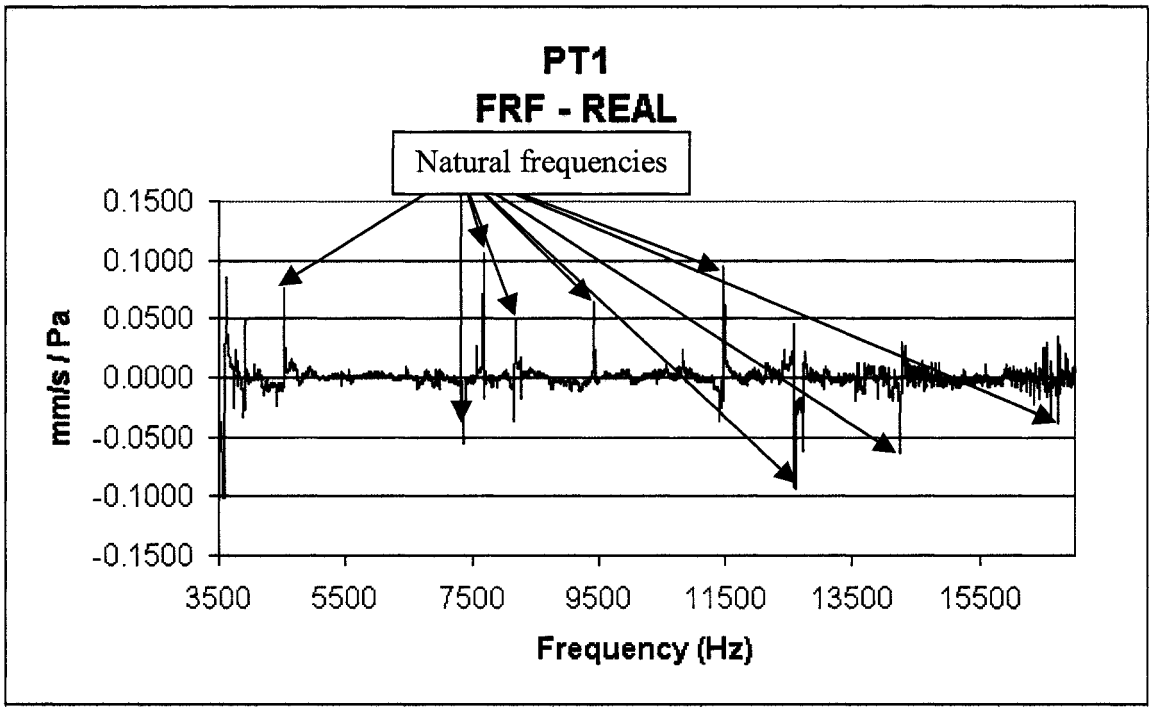

Figure 34 Example F.R.F. signal Real part for natural frequency determination

To extract the damping for each mode, the imaginary part of the signal is used since the F.R.F is in velocity over force (mobility). With the imaginary part of the signal, the two frequencies limiting the bandwidth of the resonance can be determined (w_1 and w_2). With the real part of the signal, the natural frequency of the resonance can identified (w_n). Using the following equation, the damping ratio (zeta) can be determined:

$$\zeta = \frac{(w_2 - w_1)}{2w_n} \tag{7.2}$$

All the resonances (natural frequencies) and the F.R.F Imaginary part values for every location have been tabulated in the table below (Table XII).

Table XIII

Resonances and Imaginary values for every location

Pt 1	
Resonance (Hz)	**Real Value**
4702	0.0115
7677	0.1041
8280	-0.018
9427	0.0648
10827	0.0236
11472	0.0953
12426	0.0197
14360	-0.0061
16867	0.0198

Pt 2	
Resonance (Hz)	**Real Value**
4707	0.0097
7677	0.1176
8272	0.0168
9430	0.0542
10830	0.0183
11475	0.0990
12426	-0.0105
14360	0.0083
16870	0.0152

Pt 3	
Resonance (Hz)	**Real Value**
4694	0.0105
7679	0.0355
8272	0.0167
9427	-0.0212
10835	-0.009
11472	0.0928
12434	0.0204
14373	0.0100
16865	0.0032

Pt 4	
Resonance (Hz)	**Real Value**
4683	0.0074
9398	0.0756
11478	0.0136
12431	0.0060
14341	-0.0019
16867	0.0022

Pt 5	
Resonance (Hz)	**Real Value**
4683	0.0063
7637	-0.0058
9406	0.0337
11467	-0.0076
12426	0.0064
14341	-0.0031
16748	0.0122

Pt 6	
Resonance (Hz)	**Real Value**
4680	0.0127
7631	-0.0079
9414	-0.0050
11472	0.0000
12588	-0.0424
14248	-0.0259
16756	-0.018

Pt 7	
Resonance (Hz)	**Real Value**
4683	0.0173
9411	0.1041
11483	-0.0808
12580	-0.3319
14238	-0.2105
16753	0.0427

Pt 8	
Resonance (Hz)	**Real Value**
4688	-0.0020
7634	-0.0662
9411	-0.0879
11478	-0.1363
12585	0.6843
14248	0.0138
16756	-0.0236

Pt 9	
Resonance (Hz)	**Real Value**
4686	-0.0010
7634	-0.0486
9414	-0.0444
11475	-0.0604
12585	0.3202
14246	-0.1055
16753	0.0174

As noticed, the resonances have different frequency values for every tested blade locations. The reason for this is that the setup had to be moved for every location to get focus in the mirrors of the laser vibrometer. Changing the setup introduced a small shift in the natural frequencies of the blade. Some resonances were not identified for certain locations. Either this could be due to a nodal line at that location for that particular mode shape or the displacement was so small that it could be found to be negligible.

The mode shapes were displayed using the "patch" command in MATLAB®. Each corner of the experimental mode shape represents one measure point as shown in Figure 35. The imaginary values were not modified to unity since any further analyses were performed. The experimental mode shapes are presented in the figures below with the associated analytical mode shapes (Figure 35 to Figure 47).

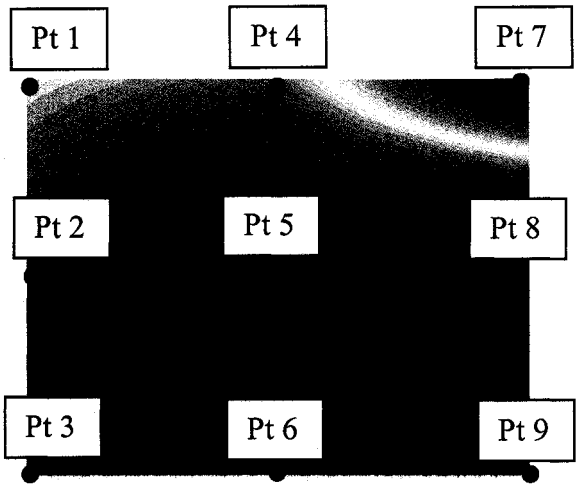

Figure 35 Exp. Mode 1 @ 4689.6 Hz

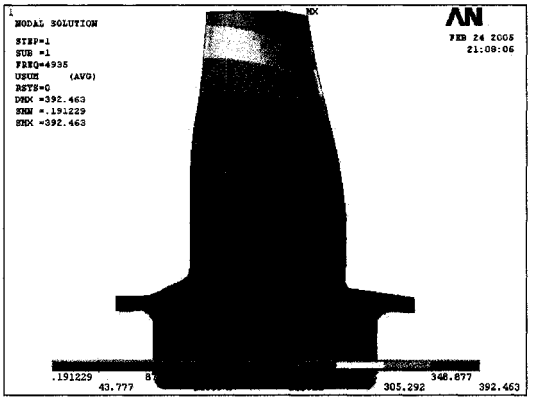

Figure 36 Mode 1 @ 4935 Hz

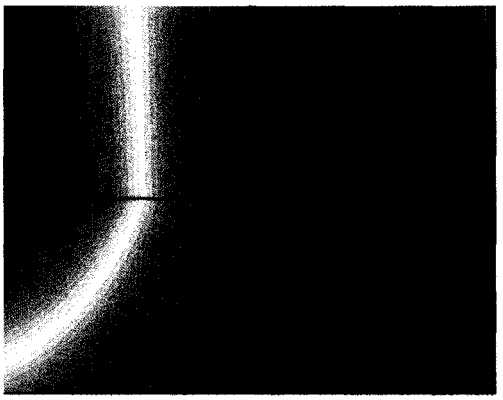

Figure 37 Exp. Mode 2 @ 7652.7 Hz

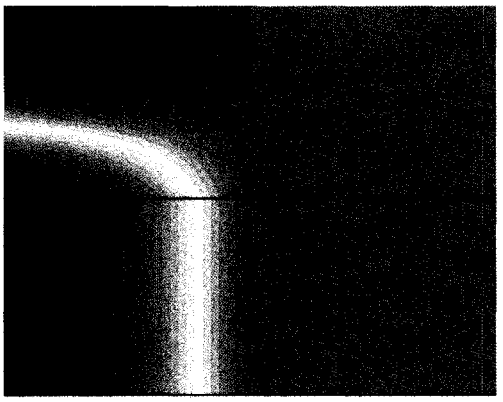

Figure 38 Exp. Mode @ 8272 Hz

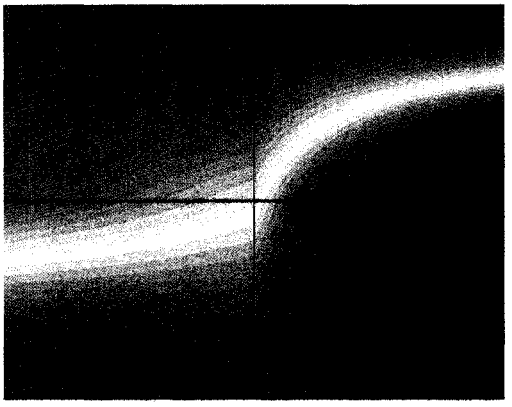

Figure 39 Exp. Mode 4 @ 9415.3 Hz

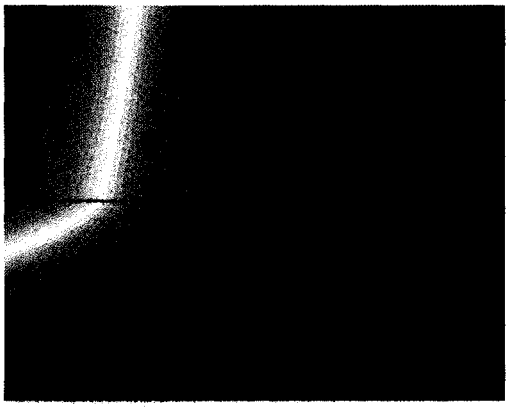

Figure 40 Exp. Mode 5 @ 10830.7 Hz

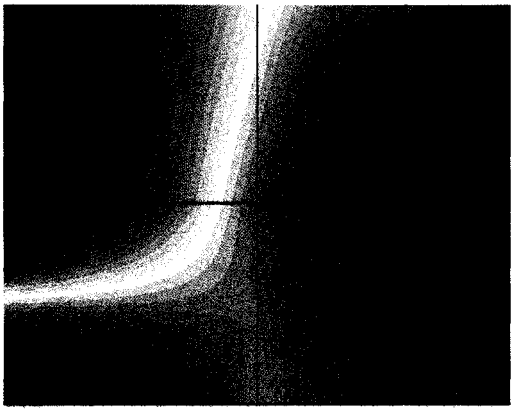

Figure 41 Exp. Mode 6 @ 11474.7 Hz

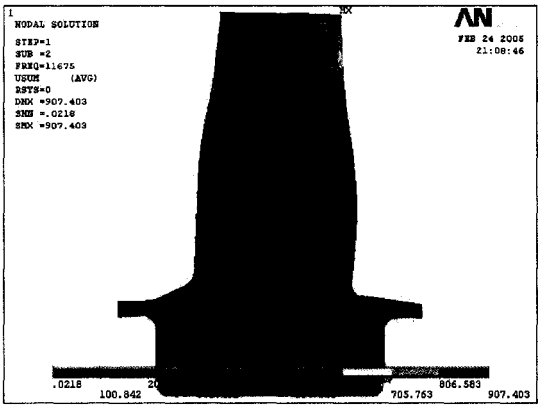

Figure 42 Mode 2 @ 11675 Hz

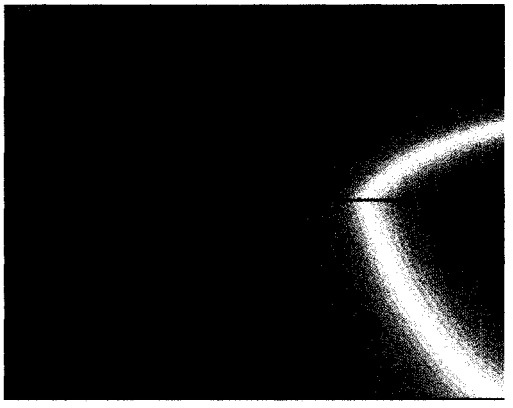

Figure 43 Exp. Mode 7 @ 12497.9 Hz

Figure 44 Exp. Mode 8 @ 14306.1 Hz

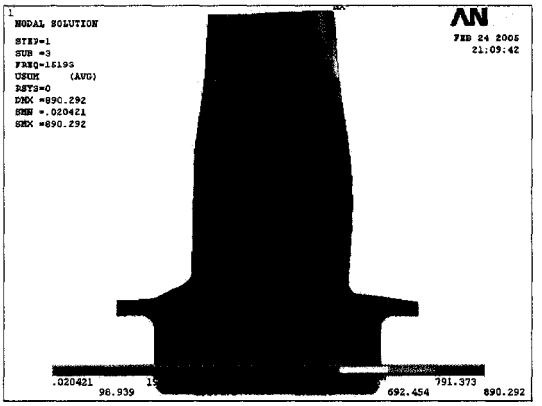

Figure 45 Mode 3 @ 15193 Hz

Figure 46 Exp. Mode 9 @ 16803.9 Hz

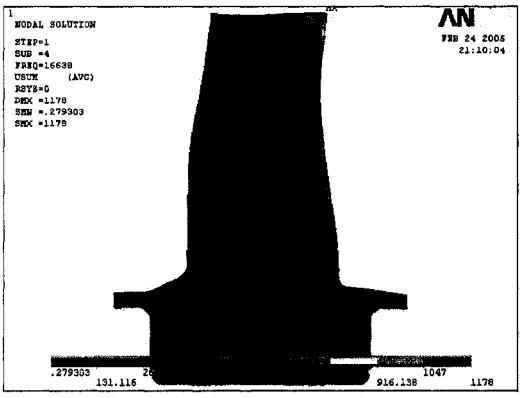

Figure 47 Mode 4 @ 16638 Hz

Nine (9) experimental mode shapes were determined during the testing. The four (4) analytical mode shapes were associated with the corresponding experimental mode shapes. The other five (5) mode shapes not associated with any experimental mode shapes were, either not present for all the locations or are due to the fixing system. The resonances frequency values were averaged for all the location and compared to the analytical resonance frequency values (Table XIII). In addition, the modal damping was extracted from the test data in the damping ratio (zeta) form. It was converted to the decrement logarithmic form using the inverse of equation 7.1.

Table XIV

Experimental and Analytical natural frequencies comparison

Experimental	Analytical	Error	Zeta	Dec. Log.
4689.6	4935	**-4.97%**	0.088%	0.0055
7652.7	N/A	**N/A**	N/A	N/A
8272	N/A	**N/A**	N/A	N/A
9415.3	N/A	**N/A**	N/A	N/A
10830.7	N/A	**N/A**	N/A	N/A
11474.7	11675	**-1.72%**	0.078%	0.0049
12497.9	N/A	**N/A**	N/A	N/A
14306.1	15193	**-5.84%**	0.056%	0.0035
16803.9	16638	**1.00%**	0.015%	0.0009

The analytical natural frequencies were determined using a friction coefficient of 0.1. Although the frequency error was less than 6 %, the modal damping values seem much below the expected range, the data cannot be completely trusted due to the lack of an excited frequency range.

Further study was made to determine the excitable frequency range of the JBL Professional Series Model No. 2425 High Frequency Speaker coupled to a Horn Model No. 2306. Using a control voltage of 0.1 Volt as a power source, the excitable frequency range of the speaker used during the experimental testing was measured using the data acquisition and the microphone. The results are plot in the power form (dB) versus frequency to determine the excitable frequency range (Figure 48).

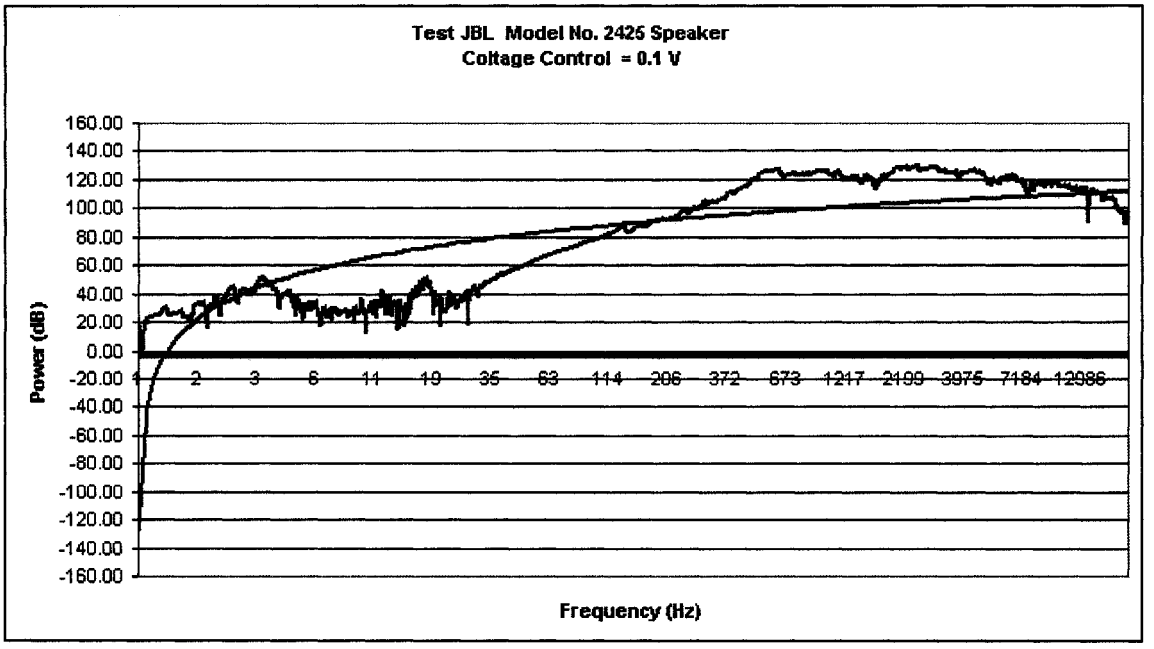

Figure 48 Excitable range on the JBL High Frequency Speaker

As demonstrated, the JBL Professional Series Model No. 2425 High Frequency Speaker coupled to a Horn Model No. 2306 has only an excitable frequency range of 500 Hz to 12 kHz. Based on the results, a negative slope in power is noticed for frequencies above 12 kHz. Furthermore, the specifications of the Professional Series Model No. 2425 High Frequency Speaker state the excitable frequencies ranges from 500 to 15 kHz (APPENDIX 5). Although there is a drop in power after 12 kHz, JBL state that the speaker is still usable for another 3 kHz. During the experimental testing, the excitable frequencies ranged from 500 Hz to 8 kHz. Therefore, not only the speaker did not have a frequency range sufficient to meet the objective of the testing but also other factors such as the frequency generator, the mixer or the amplifier could have decreased the excitable frequency range from 15 kHz to 12 kHz.

7.4 Analytical Vibratory Stress Prediction Results

Using the FLARES tool, the modal amplification factor was found for every resonance of the PWC Engine 1 HPT Blade, PWC Engine 2 HPT Blade and the PWC Engine 3 CT Blade. To determine the vibratory stress, the modal vibratory stress matrix for a particular mode was multiplied by the associated modal amplification factor. The modal vibratory stress matrix is determined by ANSYS® by using the maximum S1 or S3 strain at each node and then plotting the scaled results. The run file needed to perform a FLARES analysis in presented in the APPENDIX 6.

7.4.1 Results verification

To determine whether the FLARES results are correct, few steps must be undertaken to verify that the mode shapes and the unsteady pressure harmonics are correct.

The mode shape is generated by FLARES by reading the result file obtained from ANSYS® and compared (Figure 49 and 50). Four (4) corner nodes (Leading and trailing edges at the tip and root of the airfoil) must be specified so that the mapping between the modal analysis meshing and the CFD code meshing can be performed on the airfoil only.

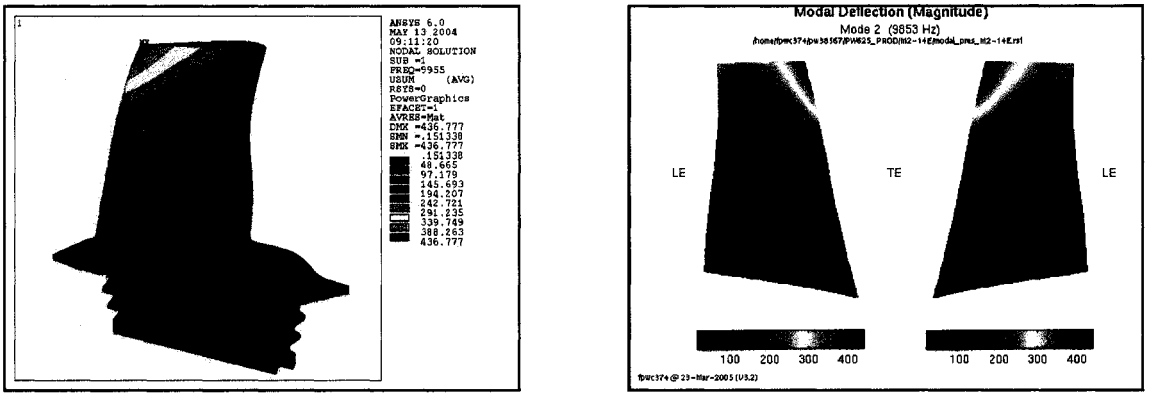

Figure 49 Mode shape comparison between ANSYS and FLARES

When the mode shape generated by FLARES is very close to the one determined by ANSYS®, it certifies that the corner nodes were chosen properly to match the CFD mesh and that the amplification factor obtained with FLARES will be correct.

It is well known that modal force is inversely proportional to the harmonic of unsteady pressure signal. Therefore, the higher the harmonic, the lower the modal force is acting on the airfoil. This has to be verified in order to certify that the aerodynamic solution is valid (Figure 50).

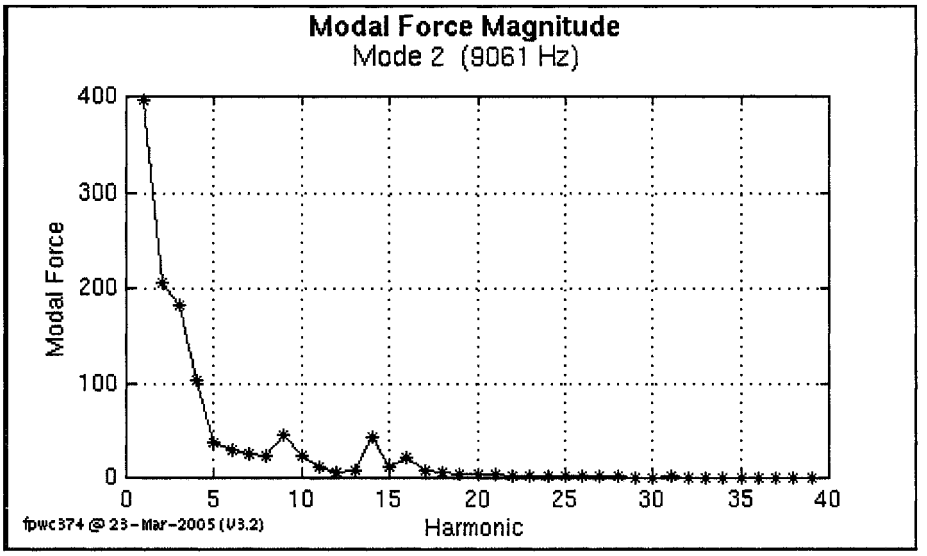

Figure 50 Modal force versus the harmonic of the unsteady pressure signal generated by FLARES

As shown in the figure above, the first harmonic of the excitation on the airfoil has a modal force higher than all the other harmonics. For the harmonics 9, 14 and 16, the error in the analytical results for these very harmonic numbers show a higher modal force than lower harmonic numbers but in reality, these harmonics would have a very small modal force value.

7.4.2 Modal amplification factor results

Based on the data reduction results presented in section 6.1, a modal amplification factor has been determined analytically for each resonance of every engine model HPT or CT blade studied.

Table XV

PWC Engine 1 HPT Blade Analytical Vibratory Stress Comparison

E6211B6 Airfoil		**FLARES Amplification Factor**	**Sensitivity**	**Predicted Vibratory Stress**	**WF Stress Error (%)**	**OA Stress Error (%)**	**EO Stress Error (%)**
Mode	**SG**						
M2-1H	3E	5.9767E-07	2.0128%	0.180109	-29.04%	53.38%	**-0.11%**
M4-2H		5.6706E-07	4.6692%	2.163107	81.60%	81.89%	**81.71%**
M2-1H	1D	5.9614E-07	2.0128%	0.839782	-27.14%	51.00%	**-1.18%**
M4-2H		5.6706E-07	4.6692%	0.446083	58.13%	72.91%	**85.37%**
M2-1H	12G	5.9645E-07	2.0128%	1.28863	16.40%	70.42%	**29.24%**
M4-2H		5.6706E-07	4.6692%	0.926066	82.45%	84.11%	**93.11%**
M2-1H	5F	6.4089E-07	2.0128%	1.048112	16.15%	68.39%	**23.26%**
M4-2H		5.6706E-07	4.6692%	1.368599	87.51%	87.88%	**87.71%**
M2-1H	7M	5.9507E-07	2.0128%	1.303144	-17.89%	76.94%	**0.68%**
M4-2H		5.6706E-07	4.6692%	1.233242	49.64%	73.53%	**91.06%**

Fixing		**FLARES Amplification Factor**	**Sensitivity**	**Predicted Vibratory Stress (ksi)**	**WF Stress Error (%)**	**OA Stress Error (%)**	**EO Stress Error (%)**
Mode	**SG**						
M2-1H	8A	6.4270E-07	2.0128%	1.115663	-17.94%	47.29%	**0.50%**
M4-2H		5.6706E-07	4.6692%	0.471448	28.37%	71.08%	**65.04%**
M2-1H	9C	6.1410E-07	2.0128%	0.819025	-6.48%	61.39%	**7.68%**
M4-2H		5.6706E-07	4.6692%	0.472401	77.13%	81.31%	**77.28%**

7.4.3 Analytical vibratory stress results interpretation

For the interpretation of the results, the first parameter to analyze is the sensitivity value obtained for each resonance. The maximum sensitivity value found was 4.67% for the whole study. This parameter dictates how much 1% of changes on any of the variables

will have an effect on the modal amplification factor calculation. By rule of thumb, if the sensitivity value is below 5%, the analysis is judged acceptable.

For the PWC Engine 1 HPT Blade, the resonance between the second mode (M2 - Trailing Edge Tip Bending) and the upstream vane passing first harmonic excitation correlates between the analytical and experimental results within 0.11% to 7.68%. Since no resonance was recorded during experimental testing, the vibratory stresses were compared at the maximum engine speed permitted and therefore off-resonance. For the same reason, no total damping value could be extracted and therefore, the total damping value was derived to achieve the minimum error possible. The total damping used to determine the vibratory stresses for the M2-1H had a logarithmic decrement value of 6.39%, which is within PWC's field of experience. The resonance between the fourth mode (M4 – Trailing Edge Second Bending) and the upstream vane passing second harmonic excitation correlates between the analytical and experimental results within 65.04% to 93.11%. The total damping value used (1.64% logarithmic decrement) was obtained for the experimental data. Compared to the other engines, the error margin is above expected for a second harmonic excitation resonance. After investigation, it was found that the steady and unsteady aerodynamic files were generated with an older code and method for this particular case. Therefore, when these aerodynamic files will be generated with the newer version of the CFD code and method, a decrease in the error between the analytical vibratory stress prediction and the experimental vibratory stress will be expected.

For the PWC Engine 2 HPT Blade, the resonance between the second mode (M2 - Trailing Edge Tip Bending) and the upstream vane passing first harmonic excitation correlates between the analytical and experimental results within 19.01% to 370.8%. The total damping value used (3.8% logarithmic decrement) was obtained for the experimental data. Since it was possible to retrieve the experimental data from the strain gage test, the analytical values were compared to values obtained from internal report, which used an older methodology to obtain the vibratory stresses. Therefore, the values

were not correlated with great confidence. The resonance between the fourth mode (M4 – Trailing Edge Second Bending) and the upstream vane passing second harmonic excitation correlates between the analytical and experimental results within 0.08% to 43.73%. The total damping value used (1.55% logarithmic decrement) was obtained for the experimental data. Compared to the other engines, the error margin is within the expected range for a second harmonic excitation resonance.

For the PWC Engine 3 CT Blade, the resonance between the second mode (M2 - Trailing Edge Tip Bending) and the upstream vane passing first harmonic excitation correlates between the analytical and experimental results within 0.02% to 14.05%. Since no resonance was recorded during experimental testing, the vibratory stresses were compared at the maximum engine speed permitted and therefore off-resonance. For the same reason, no total damping value could be extracted and therefore, the total damping value was derived to achieve the minimum error possible. The total damping used to determine the vibratory stresses for the M2-1H had a value of 13.01% logarithmic decrement, which is higher than PWC's field of experience. After investigation, it was found the CFD code could not predict the unsteady flow due to non-linear effects at high engine rotational speed. Therefore, actions have been undertaken to modify the CFD code so that it can predict these phenomenon with better accuracy. The resonance between the fourth mode (M4 – Trailing Edge Second Bending) and the upstream vane passing second harmonic excitation correlates between the analytical and experimental results within 0.87% to 52.58%. The total damping value used (0.924% logarithmic decrement) was obtained for the experimental data. Compared to the other engines, the error margin is within the expected range for a second harmonic excitation resonance.

It was determined that the lowest error margin was from the comparison between the analytical vibratory stress and the engine order (EO) vibratory stress measurement, which was expected. The waterfall value (WF) underestimates the measured vibratory stress due to marginal precision errors in the Fast Fourier Transform when converting a

time domain signal into the frequency domain. The overall value (OA) overestimated the measured vibratory stress since not only it includes the vibratory stress from the main excitation but as well as other vibratory stresses obtained from other sources of excitations. Therefore, the engine order vibratory stress value is the most accurate when considering only one particular source of excitation which is what FLARES does when calculating the vibratory stress of the an harmonic of a particular vane passing frequency.